



HAL
open science

Multiscale predictability of Cutaneous Leishmaniasis in Morocco and Tunisia through the AMO-NAO coupling and its modulation of regional rainfall

Adrià San-José, Karim Aoun, Meryem Lemrani, Mhaidi Idis, Aida Bouratbine, Richard E. Paul, Xavier Rodó

► To cite this version:

Adrià San-José, Karim Aoun, Meryem Lemrani, Mhaidi Idis, Aida Bouratbine, et al.. Multiscale predictability of Cutaneous Leishmaniasis in Morocco and Tunisia through the AMO-NAO coupling and its modulation of regional rainfall. 2024. pasteur-04559670

HAL Id: pasteur-04559670

<https://pasteur.hal.science/pasteur-04559670v1>

Preprint submitted on 25 Apr 2024

HAL is a multi-disciplinary open access archive for the deposit and dissemination of scientific research documents, whether they are published or not. The documents may come from teaching and research institutions in France or abroad, or from public or private research centers.

L'archive ouverte pluridisciplinaire **HAL**, est destinée au dépôt et à la diffusion de documents scientifiques de niveau recherche, publiés ou non, émanant des établissements d'enseignement et de recherche français ou étrangers, des laboratoires publics ou privés.



Distributed under a Creative Commons Attribution - NonCommercial - NoDerivatives 4.0 International License

Multiscale predictability of Cutaneous Leishmaniasis in Morocco and Tunisia through the AMO-NAO coupling and its modulation of regional rainfall

Authors: San-José, Adrià¹; Aoun, Karim²; Lemrani, Meryem³; Idis, Mhaidi³; Bouratbine, Aida²; Paul, Richard⁴; Rodó, Xavier^{1,5}

Affiliations:

¹ Climate and Health Program, ISGlobal, Barcelona, Spain.

² Laboratory of Medical Parasitology, biotechnology and biomolecules, LR 20-IPT-06, Institut Pasteur de Tunis, University Tunis el Manar, Tunisia.

³ Laboratory of Parasitology and Vector-Borne-Diseases, Institut Pasteur du Maroc, Casablanca 20360, Morocco.

⁴ Ecology and Emergence of Arthropod-borne Pathogens unit, Institut Pasteur, Université Paris-Cité, Centre National de Recherche Scientifique (CNRS) UMR 2000, Institut National de Recherche pour l'Agriculture, l'Alimentation et l'Environnement (INRAE) USC 1510, 75015 Paris, France.

⁵ ICREA (Catalan Institute for Research and Advanced Studies), Barcelona, Spain.

Abstract

The development of effective Early Warning Systems (EWS) for climate-driven zoonotic diseases has been hindered by a lack of predictors with adequate lead time for effective interventions. Atmosphere-Ocean coupled phenomena present predictability beyond the atmospheric deterministic limits and therefore are potentially useful climate drivers to be integrated in mathematical models. While the El Niño-Southern Oscillation (ENSO) has been used to forecast disease dynamics in equatorial and tropical regions, there is a lack of similar applications for temperate areas, likely because of the perceived unpredictability of atmospheric systems such as the North Atlantic Oscillation (NAO). This study challenges this notion by establishing a connection between the NAO and its oceanic counterpart, the Atlantic Multidecadal Oscillation (AMO), revealing common low-frequency components that strongly modulate Cutaneous Leishmaniasis (CL) in Northern Africa. We demonstrate not only short-term couplings, such as the known NAO's impact on seasonal rainfall, which subsequently affects CL incidence, but we also uncover a significant lagged effect of approximately three years on rainfall and four years on CL incidence. Our findings reveal a unified, multiscale mechanism that influences CL epidemiology across different time scales, underscoring the predictive skill for short and long term time frames, which should be integrated in CL forecasting models.

Introduction

Atmosphere-Ocean coupled phenomena and Early Warning Systems

Climate exerts a significant influence on many infectious diseases. In particular, most vector-borne diseases are influenced by prevailing weather conditions, with factors such as extrinsic incubation times, mortality and biting rates, among others, all showing sensitivity to climate variations (Caminade et al 2018). Further, the epidemiology of zoonotic diseases, known for their intricate and often delayed responses to climate, can be influenced through a multitude of complex pathways, mediated by climate-induced alterations in the landscape and vegetation, thereby impacting the population dynamics of reservoir and vector species.

Climate forcing operates across various temporal and spatial scales. Historically, infectious disease ecologists predominantly focused on examining the responses of their phenomenon of interest to local weather patterns (Stenseth et al, 2003). If strong associations emerged, this created the opportunity to make predictions days, or at a maximum weeks, ahead, depending on how slow the disease system responded to this weather forcing. As it is well known, the predictability of the atmospheric system is theoretically constrained by very short deterministic limits, making the extension of such forecasts to larger lags impossible (Tribbia et al, 1993). However, some large-scale climate processes are coupled to other more slowly-evolving systems having greater inertia (i.e. predictability), mainly in the ocean

57 compartment. An illustrative example is the ocean-atmosphere coupled phenomenon known as the El
58 Niño-Southern Oscillation (ENSO), which under certain conditions creates windows of predictability
59 months (and years) in advance (Petrova et al, 2021). In fact, ENSO has already been demonstrated to be
60 able to impact the interannual dynamics of different tropical infectious diseases, allowing for the much-
61 needed long-term predictability (Pascual et al, 2000). Under these circumstances, extended
62 predictability beyond the deterministic limits can be observed (Chen et al, 2020).

63
64 Even when theoretically possible and of potential interest to many regions and diseases, there is a
65 notable scarcity of operational early warning systems (EWS) designed to function on the necessary long
66 time-scales required and providing sufficient time for effective intervention strategies. While some
67 ENSO-based EWS exist for diseases like malaria, dengue or cholera (Pascual et al 2000, Dhiman et al
68 2017, Lowe et al 2011; Petrova et al., 2021; Siraj et al., 2014), there is very limited effort dedicated to
69 zoonotic diseases, particularly in regions beyond the tropics. Importantly, when pinpointing the climate
70 drivers behind disease transmission, merely establishing associations does not generally fit the purpose
71 in the current highly changing climate and environmental scenarios, and it therefore becomes crucial to
72 assemble a mechanistic explanation accounting for the observed effects in terms of epidemic outbreaks.
73 This is especially true when dealing with delayed, nonlinear synoptic drivers whose cascading
74 consequences can be intricate and under new conditions not covered by former data. Development of
75 dynamical models incorporating all these important covariates becomes an optimal way to proceed, in
76 the context of our current changing climate (Rodó et al., 2013).

77 78 79 80 The North-Atlantic Oscillation

81 In temperate areas, where atmospheric-ocean couplings are weaker, apparent unpredictability has
82 hindered the use of large-scale weather indices as disease predictors. In particular, the North Atlantic
83 Oscillation (NAO), a dipole pattern summarized by the surface sea-level pressure difference between
84 the Subtropical (Azores) High and the Subpolar Low (Barnston and Livezey, 1987; Luterbacher et al.,
85 2002), is often regarded as containing no climatic memory, in terms of lead time for action. This is
86 because it has an apparent featureless structure and displays very short memory (at most days or a few
87 weeks) (Fernandez et al, 2003). The NAO dominates the winter climate variability over the North
88 Atlantic and its surrounding continents (Hurrell and van Loon 1997). Despite this fact, its behavior in the
89 low-frequency range and the dynamics behind it are not fully understood yet (Greatbatch 2000; Wanner
90 et al. 2001; Marshall et al. 2001). Studies based on observational data have shown that extratropical sea
91 surface temperature (SST) anomalies could force the atmospheric circulation (Czaja and Frankignoul
92 2002). However, in general, the ocean-atmosphere coupling can lead to a limited enhanced
93 atmospheric low-frequency variability over the North Atlantic (for reviews see Kushnir et al. 2002;
94 Visbeck et al. 2003; Czaja et al. 2003). An atmospheric response to midlatitude SST anomalies in
95 combination with the oceanic gyre circulation are conceived to enhance the decadal variability of the
96 NAO (Sutton and Allen 1997; Visbeck et al. 1998; Grötzner et al. 1998; Czaja et al. 2003; Paeth et al.
97 2003). In summary, this variability shows signatures at interannual timescales, as the ones explored in
98 this study.

99 100 Cutaneous Leishmaniasis in Northern Africa

101 Cutaneous leishmaniasis (CL) is one of the main parasitic vector-borne diseases affecting human beings
102 and has an estimated annual incidence of around 1 million cases, mainly in the Americas, the
103 Mediterranean basin, the Middle East and central Asia. CL infections in humans are generally not life-
104 threatening and often resolve spontaneously, but they give rise to skin lesions and ulcers that can
105 persist for months or even years, causing significant physical, psychological and social distress among
106 affected individuals. Additionally, the disease can leave lifelong scars, leading to disability and stigma
107 (WHO).

108
109 CL is an emerging disease in Northern Africa. CL was historically limited to several oases located in arid
110 pre-Saharan zones, where it occurred sporadically leading occasionally to epidemics. However, since the
111 1980s, the geographical area of CL distribution has spread beyond its desert natural niche and an
112 increasing number of cases are observed in new endemic foci. Currently, the disease is endemo-

113 epidemic with thousands of cases reported every year in Libya, Algeria, Tunisia and Morocco. (Aoun et
114 al, 2014)

115
116 In Northern Africa, CL can be caused by three *Leishmania* species: *Leishmania (L.) infantum*, *L. major*,
117 and *L. tropica* (Aoun et al 2014). Among these, *L. major* accounts for the highest disease burden and is
118 responsible for over 90% of the cases reported in Algeria, Tunisia, and Libya. *L. major* is a zoonotic
119 parasite and is naturally sustained in northern Africa by a two-host cycle: rodents, such as the fat sand
120 rat (*Psammomys obesus*) or the gerbil (*Meriones* spp).
121 (<http://www.cfsph.iastate.edu/Factsheets/pdfs/leishmaniasis.pdf>) act as the main reservoirs, and
122 *Phlebotomus* sandflies (especially *Phlebotomus papatasi*) act as vectors. Different mammals, including
123 humans, can be infected, but most will present localized lesions and low parasitemia, thereby acting as
124 dead-end accidental hosts and being unable to further transmit the disease. Hence, CL caused by *L.*
125 *major* is referred to as Zoonotic CL (ZCL). *L. tropica*, the second most significant *Leishmania* parasite in
126 North Africa, is on the contrary mostly sustained by anthroponotic transmission chains, thus generally
127 transmitted between humans and sandflies without involving animal reservoirs (Saik et al 2022). As
128 compared to Tunisia, Algeria and Libya, the epidemiological situation of CL in Morocco is characterized
129 by a significantly higher number of cases due to *L. tropica*. This species generates an important disease
130 burden in the area between the Atlas Mountains and the Atlantic Ocean. The incidence of *L. tropica* is
131 limited to a few dozen cases in Tunisia, as in Algeria, and the parasite is suspected to be zoonotic with
132 *Ctenodactylus gondii*, a rocky mountain rodent, acting as the reservoir host (Bousslimi, 2012). Rodent
133 density, average temperature, cumulative rainfall and average relative humidity have all been shown to
134 play a role in sustaining and increasing zoonotic CL incidence (Talmoudi et al, 2017). Furthermore,
135 population acquired immunity may also play a role in modulating CL incidence (Chamakh-Ayari et al,
136 2017).

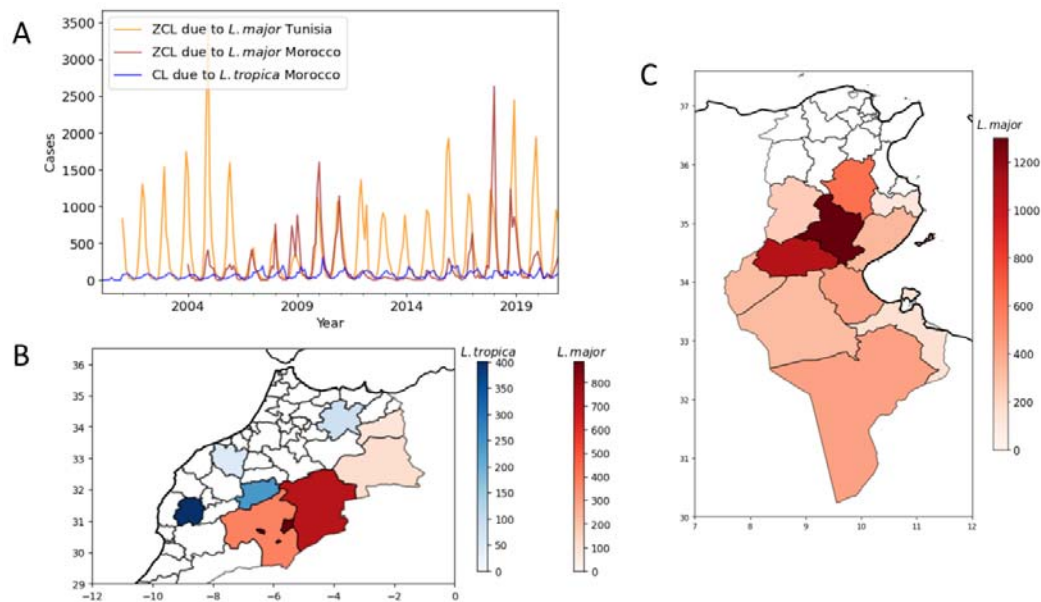
137
138 This study represents a significant advancement in the attempt to incorporate climate drivers typical of
139 the northern hemisphere into epidemic-alert systems. It has the goal of deriving a multiscale EWS, by
140 uncovering the potential for incorporating long-term predictability -up to four years in advance- for
141 anticipating CL outbreaks in Northern Africa. While keeping with short-term signatures (i.e., the NAO
142 link to seasonal rainfall), we here added a long-term modulation on the disease epidemiology defined by
143 the Atlantic Multidecadal Oscillation (AMO), as we uncovered its strong link to CL dynamics in the
144 region. To substantiate these findings, we furnished a detailed mechanistic pathway that establishes a
145 direct link between low-frequency climate forcing and the ensuing disease dynamics. Importantly, we
146 identified a unified, multiscale mechanism that operates both in the short term and over more extended
147 periods.

148 149 **Data**

150 The incidence of CL was recorded at governorate or provincial scale over a period of 17 to 23 years,
151 using databases available at regional and national levels in Tunisia and Morocco respectively. Figure 1A
152 shows the monthly incidence of CL caused by *L. major* in Tunisia along with the incidence of both *L.*
153 *major* and *L. tropica* infections in several representative Moroccan regions. Figure 1B illustrates the
154 mean yearly incidence of *L. major* and *L. tropica* in the selected provinces of Morocco. To ensure that
155 the majority of CL cases are correctly attributed at *Leishmania* species level, specific provinces were
156 selected: Errachidia, Figuig, Zagora, Jerada, and Ouarzazate being the main transmission hotspots for *L.*
157 *major*, while Azilal, Chichaoua, Settat, and Taza being the main foci of *L. tropica*. Figure 1C displays the
158 mean yearly incidence of CL caused by *L. major* in Tunisia at the governorate level.

159

160



161
162
163
164
165
166

Fig 1: (A) Monthly incidence of *L. major* infections in Tunisia and in studied provinces of Morocco, along with the incidence of *L. tropica* infections in studied regions of Morocco. (B) Mean incidence at the province level of *L. tropica* and *L. major* in Morocco (zoomed to regions with data). (C) Mean incidence at the province level of *L. major* in Tunisia.

167 Reported cases of CL in North Africa show a seasonal distribution (Figure 1A). Notably, *L. major* ZCL
168 exhibits a consistent seasonal occurrence in both Tunisia and Morocco, with case records peaking
169 around December. This seasonal pattern of ZCL is closely related to *Phlebotomus papatasi* phenology in
170 the North African region, with sandfly adult activity starting in May–June and extending to October.
171 There is a long-lasting peak of sandfly density 3 to 3.5 months before the peak of CL incidence (Chelbi et
172 al, 2007). The peak of *L. tropica* CL incidence around March is also likely attributed to sandfly vector
173 phenology but also to a longer *L. tropica* incubation period compared to that of *L. major* leading to
174 delayed onset of lesions (Aoun et al, 2022). On the other hand, Figure 1A also shows that CL incidence
175 displays clear inter-annual fluctuations. This is particularly evident with ZCL caused by *L. major*, for
176 which seasonal peaks varied from hundreds to thousands of cases according to the year (Figure 1A).

177

178 Results

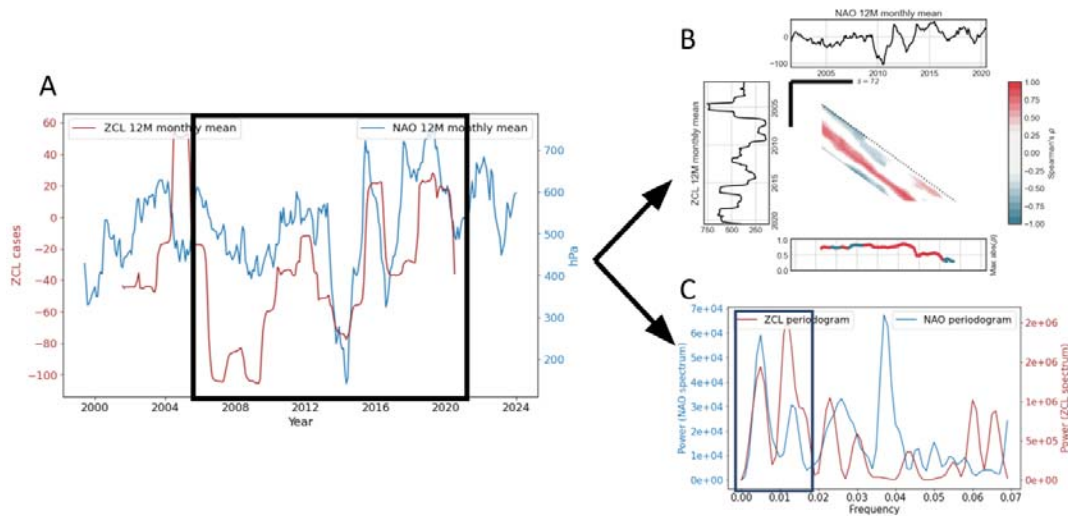
179 Multiscale analysis of the NAO

180 Precipitation in northern Africa appears to be essentially modulated in the wet season by the North
181 Atlantic Oscillation (NAO) and its associated pressure systems. Such pressure differences modulate the
182 strength of the North-Atlantic westerly winds, which are responsible for the transport of moisture
183 across the sea, and therefore impact both precipitation and temperature in extensive regions of Europe
184 and Northern Africa (Toumi et al, 2012). CL is known to be impacted by such synoptic weather patterns,
185 especially through modulation in precipitation. As such, we assessed whether the NAO index provided
186 any skill that could be used in accounting in advance for CL dynamics.

187

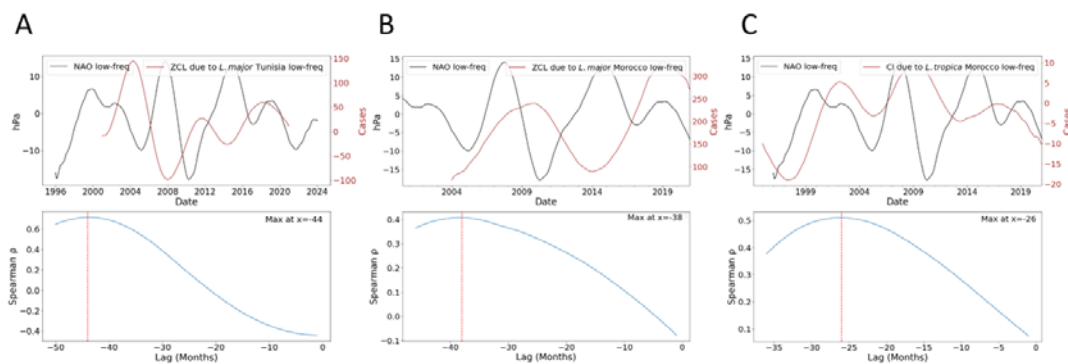
188 Analysis of the NAO effects on ZCL in Tunisia revealed strong and clear lagged low-frequency couplings
189 existing between NAO and ZCL incidence. Fig 2A displays both the NAO index and the ZCL incidence in
190 Tunisia, both smoothed with a rolling mean to remove the short-term variability. When lagged around -
191 44 months (3.5 years), a very robust coupling emerges, which is maintained throughout the whole
192 period. Fig 2B shows how stable the coupling is, by performing local-lagged Spearman correlations
193 between the time series in small windows by running a Scale-Dependent Correlation (SDC) Analysis. Fig

194 2C shows on the spectral domain this same match between dominant periods at the low-frequency end
 195 of the spectrum, thereby reinforcing the aforementioned findings.
 196
 197



198
 199 Fig 2: (A) ZCL incidence in Tunisia and NAO index, smoothed with a 12-M moving average and overlaid after lagging
 200 them -46 months. (B) SDC-Analysis of the two time series showing consistent strong couplings throughout the
 201 whole period. (C) Periodogram of both time series showing the match at the low-frequency end of the spectrum.
 202

203 To further study the low-frequency coupling existing between the NAO index and CL, a Singular
 204 Spectrum Analysis (SSA) was applied to both the NAO and the three country-wise aggregated CL time
 205 series (*L. major* in Tunisia, *L. major* in Morocco and *L. tropica* in Morocco). Of relevance, a common low-
 206 frequency component emerged from the four aforementioned SSA decompositions with a period of
 207 around 7-10 years (Figure 3).
 208



209
 210 Fig 3: Low-frequency coupling NAO-CL. (A) For ZCL due to *L. major* in Tunisia. Up: Overlaid low-frequency
 211 components. Down: Cross-correlation analysis, showing a peak at -44 months (p -value<0.05). (B) For ZCL due to *L.*
 212 *major* in Morocco. Up: Overlaid low-frequency components. Down: Cross-correlation analysis, showing a peak at -
 213 38 months (p -value<0.1; n being shorter) (C) For CL due to *L. tropica* in Morocco. Up: Overlaid low-frequency
 214 components. Down: Cross-correlation analysis, showing a peak at -26 months (p -value<0.05).
 215

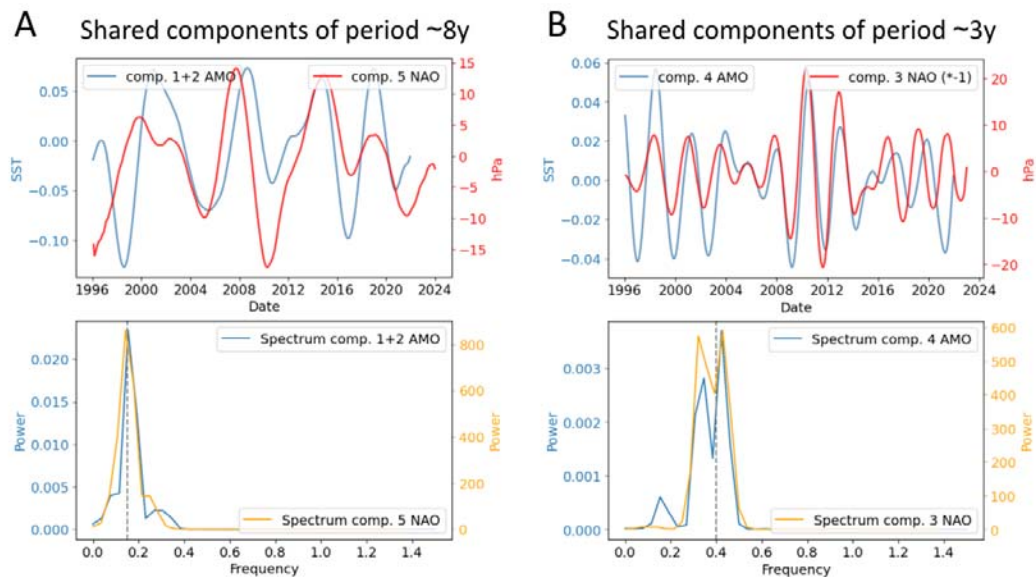
216 For the three CL situations, cross-correlation analyses between the low-frequency NAO and the low-
 217 frequency CL time series resulted in a unimodal function with a peak at -44 months (Tunisia *L. major*, p -
 218 value<0.05), -38 months (Morocco *L. major*, p -value<0.1; n being shorter) and -26 months (Morocco *L.*
 219 *tropica*, p -value<0.05) (Fig. 3). Similar lags, of around 3-3.5 years therefore naturally arose in Tunisia and
 220 Morocco for *L. major*. In parallel, a strong NAO-*L. tropica* match also emerged, despite the latter being
 221 at shorter lags.
 222

223 Given the long lead times obtained, we proceeded to investigate the role and associated signatures of
 224 the Atlantic Multi-Decadal Oscillation (AMO), a coherent mode of interdecadal climate variability

225 occurring in the North Atlantic Ocean with a fundamental estimated period of 60-80 years, based upon
226 the average anomalies of SSTs in the North Atlantic basin.

227
228 To this end, a SSA was again computed but now for the AMO index to have it decomposed into its main
229 modes of variability. Cross-inspection with the former SSA executed over the NAO showed common
230 low-frequency covariating components between the two phenomena. In fact, such decompositions
231 clearly display that the NAO-AMO coupling effectively operates synchronously across various temporal
232 scales. The characteristic period of 7-10 years previously found in all CL time series and the NAO index,
233 similarly shows up in the AMO (Figure 4A). Additionally, it became clear there exists a strong coherency
234 between the 3rd component of the NAO and the 4th component of the AMO index, both showing a
235 similar frequency peak at periods between around 2 - 3.5 years (Fig. 4). Collectively, these components
236 elucidate approximately 17% and 7% of the AMOs and NAOs original variance, respectively.

237
238



239
240 Fig 4. NAO-AMO coupling. (A) Shared components with a period of around 8y. (Up) Superposition of the 5th NAO
241 component and the 1+2 AMO components (Spearman's $\rho=0.48$, $p_value<0.05$). (Down) Overlaid Spectral
242 decomposition of such NAO and AMO 8y components (B) Shared components of period of around 3y (Up)
243 Superposition of the 3rd NAO component with the 4th AMO component (Spearman's $\rho=0.53$, $p_value <0.05$).
244 (Down) Overlaid spectral decomposition of such NAO and AMO 3y components.

245

246 The overlaid ~8-year reconstructed components of both the leishmania parasites and the climate indices
247 under investigation (namely, the NAO, AMO, *L. major* Tunis, *L. major* Morocco, *L. tropica* Morocco) can
248 be seen in Fig S1.

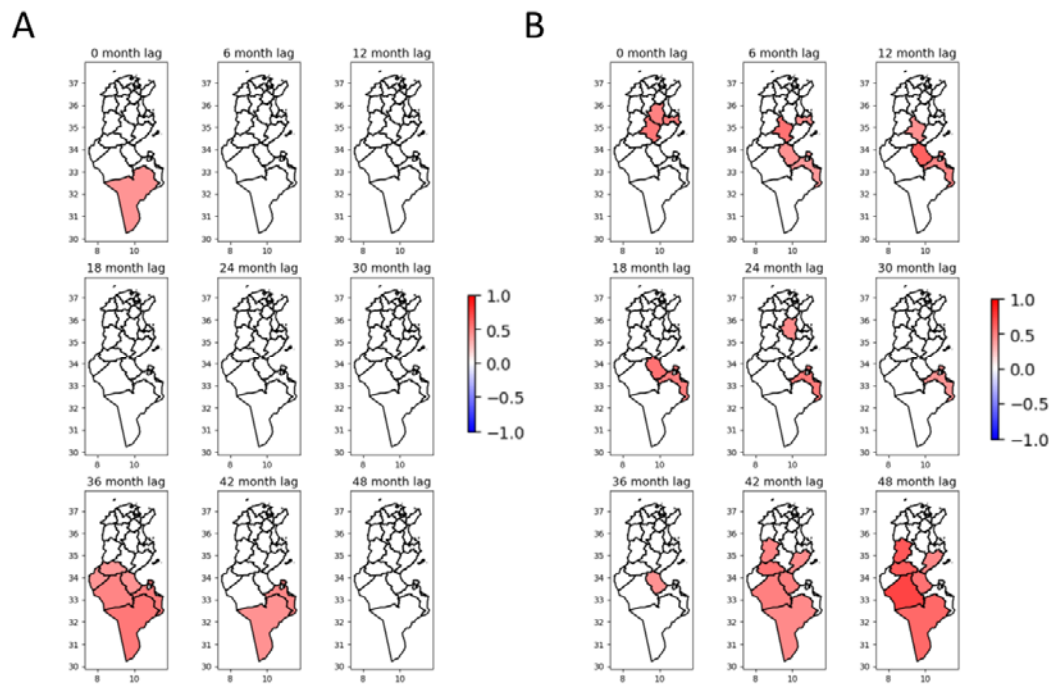
249

250

251 Short-term responses

252 As previously discussed, the NAO modulates the strength of the westerly winds, which are responsible
253 for carrying moisture across the Atlantic, and therefore they seasonally impact both precipitation and
254 temperature in Europe and Northern Africa. It is furthermore surprising to find a large lagged effect
255 given that the NAO instead has an instant effect on precipitation and quickly loses predictability
256 (Wunsch, 1999). Indeed, at these very short time scales ZCL in Tunisia is seen to be strongly associated
257 with synoptic weather events displaying a dipole linked to the NAO phenomenon through the Açores
258 pole (Fig S3), despite being also partly related to the Scandinavian Mode (Wang and Tang, 2020). Its
259 associated skill can be traced back to a maximum of 6 months in the form of leading sea-level pressure
260 anomalies (Fig S3).

261 To further delve into the climatic forcing mechanisms operating on ZCL dynamics, we zoomed in and
262 regionalized the analyses in Tunisia. We identified an expected significant short-term coupling between
263 the NAO and precipitation raw values (not shown), which also showed up after applying a 12-month
264 smoothing filter (Fig 5A). However, apart from the short-term coupling, the associations at longer lags
265 previously identified similarly showed up (Fig 5A).
266
267



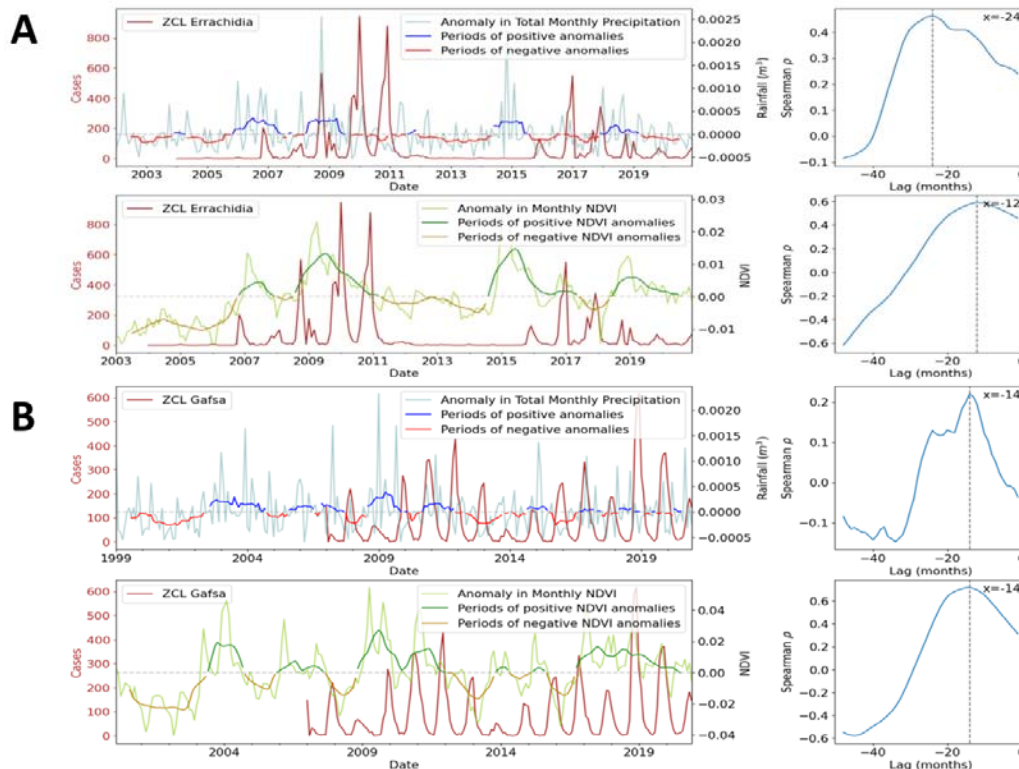
268 Fig. 5: (A) Significant full series correlations (p -value < 0.05) of NAO vs. Rainfall (smoothed with 12-mo moving
269 windows) in Tunisia at the province level from 2007 to 2021. (B) Significant correlations (p -value < 0.05) NAO vs ZCL
270 (smoothed with a 12-mo moving average) in Tunisia at the provincial level for the period 2007-2021
271
272
273

274 In the previous analysis a maximum low-frequency NAO-ZCL coupling was found for Tunisia with a 44
275 months delay (Fig 2A). We now obtained a maximum NAO-Precipitation coupling located at 36 months
276 delay, therefore around 1 year before that obtained for the NAO-ZCL, thereby reinforcing our previous
277 findings and showcasing how precipitation mediates in the cascade effects of NAO on ZCL in Tunisia.
278

279 We proceeded to perform the same analyses but, now instead, directly between the NAO and ZCL. In a
280 higher spatial resolution domain, we again obtained evidence regarding the existence of a strong NAO-
281 ZCL coupling at around -44 months lag, manifesting especially in the middle and southern part of
282 Tunisia, where we also saw the best couplings with precipitation. (Fig 5A, 5B)
283

284 The relationship between NAO and precipitation in Morocco is less direct and evident compared to the
285 situation in Tunisia (Figs S5, S6).
286

287 Local precipitation impacts ZCL short-frequency dynamics in both countries (Fig. 6). At the Governorate
288 level / Wilaya level, ZCL and precipitation tend to show a maximum coupling at around a year lag.
289 Interestingly, the normalized difference vegetation index (NDVI), known to respond tightly to rainfall in
290 these types of climates, displayed higher correlations with ZCL at slightly shorter lags. Figure 9 shows a
291 noticeable example of such coupling for Errachidia (Morocco) and Gafsa (Tunisia).
292
293
294
295



296

297

298

299

300

301

302

303

304

305

306

307

308

309

310

311

312

313

314

315

316

317

318

319

320

321

322

323

324

325

326

327

328

Fig. 6. ZCL-Rainfall couplings (up) and ZCL-NDVI couplings (down) -and cross-correlation analyses (CCF), right- for (A) Errachidia (Morocco) and (B) Gafsa (Tunisia). All original rainfall, NDVI and ZCL time series are shown (in light blue, light green and brown). The graphs also display the result of 12-mo moving filter on the climatic and environmental time series, which serve to illustrate periods of positive anomalies (in blue for precipitation and green for NDVI) and negative anomalies (in red for precipitation and yellow for NDVI). CCFs are performed after applying a 12-mo moving filter to all time series to remove short term variability. The correlation peaks for the cross-correlations from Errachidia all pass a significance test at $\alpha=0.05$. For Gafsa, and mainly because the timeseries is shorter, the cross-correlation peak with rainfall doesn't pass a test ($p_{\text{value}} < 0.1$) but it does with NDVI.

Discussion

Very few studies have attempted to investigate the inter-annual modulation of CL and associate it to external forcings. One seminal study identified 3y cycles in CL data from Costa Rica and hypothesized them to be connected to the El Niño Southern Oscillation (ENSO) phenomenon (Chaves et al, 2006). A shared frequency peak was identified between CL incidence and the ENSO MEI index, but the study did not provide a detailed mechanistic explanation of how the atmosphere-ocean coupling takes place from the source region in the equatorial SST and the local CL dynamics in Costa Rica. As such, the exact mechanistic cascading pathway underlying the findings remained elusive.

In this study, instead, we proved that despite the distance between Morocco and Tunisia, and the large known differences between *L. major* and *L. tropica* epidemiological cycles, all the studied different CL disease situations in North-Africa show strong low-frequency components being shared with the NAO. In fact, such couplings take place at very similar lags for the two *L. major* situations, but at a different lag for *L. tropica*. This apparent discrepancy should not be surprising and reinforces these findings. *L. tropica* represents a non-zoonotic form of CL, that does not appear to operate through an animal reservoir. Therefore, we hypothesize that it presumably responds faster to the same extrinsic climatic stressor, which would explain the shorter lags found. Overall, we inferred that CL inter-annual dynamics are governed by a large-scale climate synoptic pattern, which likely operates along with population acquired immunity to determine the final low-frequency patterns of the CL time series (Chamakh-Ayari et al, 2017).

Overall, we identified two shared components between the NAO and the AMO illustrating that both are showing responses to the same climatic process. Therefore, from a mechanistic perspective, a unique

329 unified mechanism can explain both the multiscale short-term and long-term relationships between
330 climate and ZCL epidemiology in Northern Africa.

331
332 Regarding the exact pathways by which such large-scale indices locally affect transmission, we identified
333 a strong modulation of precipitation in Tunisia, both instantaneous and at 3 years lag. On the latter it is
334 important to say that such a 3-year lag is around one year before the maximum couplings appear with
335 respect to the disease (which manifest around a 4-year lag). This one-year difference between the
336 cascading effects of precipitation on the disease (i.e., before effects show up in ZCL incidence) was also
337 independently identified in Fig 9, thereby reinforcing our findings. Furthermore, by integrating data
338 from vegetation, which strongly couples to ZCL incidence, we found evidence that supports the notion
339 that vegetation plays a key role in sustaining and increasing zoonotic CL incidence. These results are in
340 line with those of other studies showing that the incidence of ZCL in central Tunisia increased
341 significantly when there was an increase in rainfall lagged by 12 to 14 months (Toumi et al, 2012). They
342 are also in accordance with results of other studies that found that the occurrence of ZCL is related to
343 rodents' density but lagged 2 months (Talmoudi et al, 2017). In fact, higher rainfall is expected to result
344 in increased density of vegetation, particularly for chenopods, a halophytic plant that constitutes the
345 exclusive food source of *P. obesus*. Presumably, following a high density of *P. obesus*, the source of *L.*
346 *major* transmissible from the rodents to blood-feeding female sand flies could lead to a higher
347 probability of transmission to humans over the next season.

348
349 In Morocco, the NAO did not so clearly appear to modulate precipitation, especially when aggregating
350 data from the whole country. Morocco's unique and complex geographical position, being in a fringe
351 topographic region separated by the Atlas Mountains, may be behind the fainter signature -albeit also
352 significant- obtained with CL. This mountain range is responsible for the distinct manifestation of
353 precipitation patterns on either side, ultimately being influenced by diverging interactions with the
354 Atlantic moist winds and steep topography. The nonlinearities in the observed Morocco's ZCL response
355 to the NAO could also be due to these more complex, multifaceted pathways by which the NAO
356 modulates climate in northern Africa.

357 358 **Conclusions**

359
360 The AMO low-frequency oceanic pattern in the North Atlantic modulates the low-frequency dynamics of
361 ZCL epidemiology in North Africa. Its fundamental role can explicitly be traced to the cascading effects
362 connecting the long-term SST changes in the North Atlantic to the ZCL dynamics. In particular, we could
363 show how some of the main modes of variability of the AMO are transferred via the NAO. Physically,
364 this means that variations in the SST anomalies of the Atlantic Ocean may operate in the form of large-
365 scale changes in synoptic weather conditions subsequently affecting the moist westerly winds patterns
366 over the Atlantic. This in turn creates changes in precipitation across North Africa that can be traced to
367 ultimately affect CL incidence through cascading effects in vegetation.

368 A multi-scale prediction system such as the one described in this study, that can operate at both long
369 (roughly 4 years) and short (6 months) having the NAO and the AMO as the sources of climatic memory,
370 therefore predictability, has never been built before. Importantly our results identify a unique multiscale
371 mechanism accounting for both short-term and long-term dynamics, that could be promptly integrated
372 to provide an alert system for the different types of cutaneous leishmaniasis in the region.

373 374 375 **Methods**

376
377 Scale-Dependent Correlation (SDC) analysis is an optimal method for identifying dynamical couplings in
378 short and noisy time series (Rodo et al, 2006). In general, Spearman correlations between incidence and
379 a meteorological time series assess whether there is a monotonic relation between the variables. SDC
380 analysis was specifically developed to study transitory associations that are local in time at a specified
381 temporal scale corresponding to the size of the time intervals considered (s). The two-way
382 implementation (TW-SDC) is a bivariate method that computes non-parametric Spearman rank
383 correlations between two time series, for different pairs of time intervals along these series. Different
384 window sizes (s) can be used to examine increasingly finer temporal resolution. Significance is assessed
385 with a non-parametric randomization test. For the baseline test, SDC calculates Spearman correlations

386 (at $\alpha=0.05$) between two white-noise time series at each fragment size s for a non-parametric
387 permutation test. The indices of the series are randomly re-ordered, breaking their temporal shape. This
388 permutation test enables a first estimate of the probability of finding significant spurious correlations,
389 and it can thus be used as a non-parametric significance test for pairs of any length for the time series of
390 interest. (The code in Python for Scale-Dependent Correlation Analysis (SDC) developed by X.R. can be
391 found at <https://github.com/AlFontal/sdcpy>.)
392

393 Singular spectrum analysis (SSA) (Ghil et al 2002, Vautard et al 1992) was applied to separate different
394 orthogonal components in both the CL time series and the climate ones. SSA involves the spectral
395 decomposition (eigenvalues and corresponding eigenvectors) of a covariance matrix obtained by lagging
396 the time series data for a prescribed number of lags M called the embedding dimension. There are two
397 crucial steps in this analysis for which there are no formal results but useful rules of thumb: one is the
398 choice of M ; the other is the grouping of the eigenvectors to define the specific major components and
399 reconstruct them. Typically, the grouping of the eigencomponents is based on the similarity and
400 magnitudes of the eigenvalues, their power (variance of the data they account for), and the peak
401 frequency of resulting reconstructed components (RC). For the selection of the embedding dimension
402 one general strategy is to choose it so that at least one period of the lowest frequency component of
403 interest can be identified, that is $M \geq 2\pi f_s / f_r$, where f_s is the sampling rate and f_r is the minimum
404 frequency. Another strategy is that M be large enough so that the M -lagged vector incorporates the
405 temporal scale of the time series that is of interest. The larger the M , the more detailed the resulting
406 decomposition of the signal. In particular, the most detailed decomposition is achieved when the
407 embedding dimension is approximately equal to half of the total signal length. A compromise must be
408 reached, however, as a large M implies increased computation, and too large a value may produce a
409 mixing of components. SSA, given its data-adaptive nature and orthogonal decomposition approach, can
410 be used as an alternative smoothing method to moving averages, which is more flexible and robust, and
411 also deals better with non-stationary noisy time series (Ghil et al., 2002).

412 Rainfall in semi-arid regions typically exhibits a lot of stochasticity. We applied moving averages in some
413 situations to extract lower-frequency components. In such instances, and also in the analysis of low-
414 frequency components, given that both series become more autocorrelated and their number of
415 degrees of freedom decreases, we calculated p -values by correcting by the effective degrees of
416 freedom. In particular, we employed a bootstrap approach to assess their significance. To compute the
417 distribution of resulting correlation coefficients from which we determined significance, we repeatedly
418 randomized the smoothed time series while keeping original autocorrelation.

419 To study responses in vegetation to rainfall variability ultimately impacting CL, we used the normalized
420 difference vegetation index (NDVI). NDVI is a remote sensing measurement used to assess the density
421 and health of vegetation. It calculates the difference between near-infrared (which vegetation strongly
422 reflects) and red light (which vegetation absorbs) from satellite or aerial imagery, providing a numerical
423 indicator that can be used to monitor plant growth, vegetation cover, and biomass production.

424
425

426 Bibliography

- 427
- 428 1. Aoun K, Bouratbine A. Cutaneous Leishmaniasis in North Africa: a review. *Parasite*. 2014;21:14.
429 doi:10.1051/parasite/2014014
- 430 2. Aoun K, Kalboussi Y, Ben Sghaier I, et al. Assessment of Incubation Period of Cutaneous
431 Leishmaniasis due to *Leishmania major* in Tunisia. *Am J Trop Med Hyg*. 2020;103(5):1934-1937.
432 doi:10.4269/ajtmh.20-0439
- 433 3. Barnston AG, Livezey RE. Classification, Seasonality and Persistence of Low-Frequency
434 Atmospheric Circulation Patterns. *Mon Weather Rev*. 1987;115(6):1083-1126.
435 doi:10.1175/1520-0493(1987)115<1083:CSAPOL>2.0.CO;2
- 436 4. Ben-Ayed S, Ben-Abda I, Bousslimi N, Aoun K, Bouratbine A. Natural Infection of North African
437 Gundi (*Ctenodactylus gundi*) by *Leishmania tropica* in the Focus of Cutaneous Leishmaniasis,
438 Southeast Tunisia. *Am J Trop Med Hyg*. 2012;86(6):962-965. doi:10.4269/ajtmh.2012.11-0572
- 439 5. Caminade C, McIntyre KM, Jones AE. Impact of recent and future climate change on
440 vector-borne diseases. *Ann N Y Acad Sci*. 2019;1436(1):157-173. doi:10.1111/nyas.13950

- 441 6. Chamakh-Ayari R, Chenik M, Chakroun AS, Bahi-Jaber N, Aoun K, Meddeb-Garnaoui A.
442 Leishmania major large RAB GTPase is highly immunogenic in individuals immune to cutaneous
443 and visceral leishmaniasis. *Parasit Vectors*. 2017;10(1):185. doi:10.1186/s13071-017-2127-3
- 444 7. Chaves LF, Pascual M. Climate Cycles and Forecasts of Cutaneous Leishmaniasis, a Nonstationary
445 Vector-Borne Disease. *PLoS Med*. 2006;3(8):e295. doi:10.1371/journal.pmed.0030295
- 446 8. Chelbi I, Derbali M, Al-Ahmadi Z, Zaafourri B, El Fahem A, Zhioua E. Phenology of Phlebotomus
447 papatasi (Diptera: Psychodidae) relative to the seasonal prevalence of zoonotic cutaneous
448 leishmaniasis in central Tunisia. *J Med Entomol*. 2007;44(2):385-388. doi:10.1603/0022-
449 2585(2007)44[385:poppdp]2.0.co;2
- 450 9. Chen HC, Tseng YH, Hu ZZ, Ding R. Enhancing the ENSO Predictability beyond the Spring Barrier.
451 *Sci Rep*. 2020;10(1):984. doi:10.1038/s41598-020-57853-7
- 452 10. Czaja A, Frankignoul C. Observed Impact of Atlantic SST Anomalies on the North Atlantic
453 Oscillation. *J Clim*. 2002;15(6):606-623. doi:10.1175/1520-
454 0442(2002)015<0606:OIOASA>2.0.CO;2
- 455 11. Czaja A, Robertson AW, Huck T. The role of Atlantic Ocean-atmosphere coupling in affecting
456 North Atlantic oscillation variability. In: ; 2003:147-172. doi:10.1029/134GM07
- 457 12. Dhiman RC, Sarkar S. El Niño Southern Oscillation as an early warning tool for malaria outbreaks
458 in India. *Malar J*. 2017;16(1):122. doi:10.1186/s12936-017-1779-y
- 459 13. Fernández I, Hernández CN, Pacheco JM. Is the North Atlantic Oscillation just a pink noise?
460 *Physica A: Statistical Mechanics and its Applications*. 2003;323:705-714. doi:10.1016/S0378-
461 4371(03)00056-6
- 462 14. Ghil M, Allen MR, Dettinger MD, et al. ADVANCED SPECTRAL METHODS FOR CLIMATIC TIME
463 SERIES. *Reviews of Geophysics*. 2002;40(1). doi:10.1029/2000RG000092
- 464 15. Greatbatch RJ. The North Atlantic Oscillation. *Stochastic Environmental Research and Risk
465 Assessment*. 2000;14(4):0213-0242. doi:10.1007/s004770000047
- 466 16. HURRELL JW, VAN LOON H. Decadal Variations in Climate Associated with the North Atlantic
467 Oscillation. *Clim Change*. 1997;36(3/4):301-326. doi:10.1023/A:1005314315270
- 468 17. El Idrissi Saik I, Benlabsir C, Fellah H, Lemrani M, Riyad M. Transmission patterns of Leishmania
469 tropica around the Mediterranean basin: Could Morocco be impacted by a zoonotic spillover?
470 *PLoS Negl Trop Dis*. 2022;16(1):e0010009. doi:10.1371/journal.pntd.0010009
- 471 18. Jones CD, Cox PM. Constraints on the temperature sensitivity of global soil respiration from the
472 observed interannual variability in atmospheric CO₂. *Atmospheric Science Letters*. 2001;2(1-
473 4):166-172. doi:10.1006/asle.2001.0044
- 474 19. Kushnir Y, Robinson WA, Bladé I, Hall NMJ, Peng S, Sutton R. Atmospheric GCM Response to
475 Extratropical SST Anomalies: Synthesis and Evaluation*. *J Clim*. 2002;15(16):2233-2256.
476 doi:10.1175/1520-0442(2002)015<2233:AGRTES>2.0.CO;2
- 477 20. Lowe R, Bailey TC, Stephenson DB, et al. Spatio-temporal modelling of climate-sensitive disease
478 risk: Towards an early warning system for dengue in Brazil. *Comput Geosci*. 2011;37(3):371-381.
479 doi:10.1016/j.cageo.2010.01.008
- 480 21. Marshall J, Johnson H, Goodman J. A Study of the Interaction of the North Atlantic Oscillation
481 with Ocean Circulation. *J Clim*. 2001;14(7):1399-1421. doi:10.1175/1520-
482 0442(2001)014<1399:ASOTIO>2.0.CO;2
- 483 22. Paeth H, Latif M, Hense A. Global SST influence on twentieth century NAO variability. *Clim Dyn*.
484 2003;21(1):63-75. doi:10.1007/s00382-003-0318-4
- 485 23. Pascual M, Rodó X, Ellner SP, Colwell R, Bouma MJ. Cholera Dynamics and El Niño-Southern
486 Oscillation. *Science (1979)*. 2000;289(5485):1766-1769. doi:10.1126/science.289.5485.1766
- 487 24. Petrova D, Rodó X, Sippy R, et al. The 2018–2019 weak El Niño: Predicting the risk of a dengue
488 outbreak in Machala, Ecuador. *International Journal of Climatology*. 2021;41(7):3813-3823.
489 doi:10.1002/joc.6744
- 490 25. Rodó X, Pascual M, Doblas-Reyes FJ, et al. Climate change and infectious diseases: Can we meet
491 the needs for better prediction? *Clim Change*. 2013;118(3-4):625-640. doi:10.1007/s10584-013-
492 0744-1
- 493 26. Rodó X, Rodríguez-Arias MÀ. A new method to detect transitory signatures and local time/space
494 variability structures in the climate system: the scale-dependent correlation analysis. *Clim Dyn*.
495 2006;27(5):441-458. doi:10.1007/s00382-005-0106-4

- 496 27. Rodríguez-Arias MÀ, Rodó X. A primer on the study of transitory dynamics in ecological series
497 using the scale-dependent correlation analysis. *Oecologia*. 2004;138(4):485-504.
498 doi:10.1007/s00442-003-1464-4
- 499 28. Siraj AS, Santos-Vega M, Bouma MJ, Yadeta D, Carrascal DR, Pascual M. Altitudinal Changes in
500 Malaria Incidence in Highlands of Ethiopia and Colombia. *Science (1979)*. 2014;343(6175):1154-
501 1158. doi:10.1126/science.1244325
- 502 29. Talmoudi K, Bellali H, Ben-Alaya N, Saez M, Malouche D, Chahed MK. Modeling zoonotic
503 cutaneous leishmaniasis incidence in central Tunisia from 2009-2015: Forecasting models using
504 climate variables as predictors. *PLoS Negl Trop Dis*. 2017;11(8):e0005844.
505 doi:10.1371/journal.pntd.0005844
- 506 30. Toumi A, Chlif S, Bettaieb J, et al. Temporal Dynamics and Impact of Climate Factors on the
507 Incidence of Zoonotic Cutaneous Leishmaniasis in Central Tunisia. *PLoS Negl Trop Dis*.
508 2012;6(5):e1633. doi:10.1371/journal.pntd.0001633
- 509 31. Tribbia J, Baumhefner D. On the Problem of Prediction Beyond the Deterministic Range. In:
510 *Prediction of Interannual Climate Variations*. Springer Berlin Heidelberg; 1993:251-264.
511 doi:10.1007/978-3-642-76960-3_14
- 512 32. Vautard R, Yiou P, Ghil M. Singular-spectrum analysis: A toolkit for short, noisy chaotic signals.
513 *Physica D*. 1992;58(1-4):95-126. doi:10.1016/0167-2789(92)90103-T
- 514 33. Visbeck M, Chassignet EP, Curry RG, Delworth TL, Dickson RR, Krahnmann G. The ocean's
515 response to North Atlantic Oscillation variability. In: ; 2003:113-145. doi:10.1029/134GM06
- 516 34. Visbeck MH, Hurrell JW, Polvani L, Cullen HM. The North Atlantic Oscillation: Past, present, and
517 future. *Proceedings of the National Academy of Sciences*. 2001;98(23):12876-12877.
518 doi:10.1073/pnas.231391598
- 519 35. Wanner H, Brönnimann S, Casty C, et al. North Atlantic Oscillation – Concepts And Studies. *Surv*
520 *Geophys*. 2001;22(4):321-381. doi:10.1023/A:1014217317898
- 521 36. Wunsch C. The Interpretation of Short Climate Records, with Comments on the North Atlantic
522 and Southern Oscillations. *Bull Am Meteorol Soc*. 1999;80(2):245-255. doi:10.1175/1520-
523 0477(1999)080<0245:TIOSCR>2.0.CO;2

524 525 526 **Acknowledgements**

527
528 The authors acknowledge Drs Latifa Maazaoui and Kaouther Hrabech from the Tunisian Ministry of
529 Health for their precious help in the collection of CL data.

530 A.SJ was supported by a fellowship from “la Caixa” Foundation, Spain (ID 100010434, fellowship code
531 LCF/BQ/DR19/11740017). A. SJ and X.R. acknowledge the support from the grant CEX2018-000806-S
532 funded by MCIN/AEI/10.13039/501100011033 and support from the Generalitat de Catalunya through
533 the CERCA Program.

534
535
536